Design Proposal for Silicon Photonics Design Course

Calisto Ruiz (calistor2)

***Abstract*—The following entails the design parameters, waveguide geometry, and layout for implementing Mach-Zehdner interferometers and ring resonators. Included are essential formulas, explanation of design choices, and simulation data qualifying the designs.**

***Index Terms*—Silicon photonics, Mach-Zehder interferometer.**

I. Introduction

THE Mach-Zehnder interferometer (MZI) and ring resonator are critical components in Silicon Photonics, as they can be used in a variety of applications such as wavelength-division multiplexing, optical switches, and electro-optical modulators [1]. By tuning the geometry of the devices, the optical filtering properties can be precisely tuned to add or drop certain wavelengths. The following entails the design variations employed and the fabricated device performance.

II. Theory

A. Mach Mach-Zehnder Interferometer

A MZI works by splitting an incoming beam into two parts, sending each part down separate paths, and then recombining the beams. Based on the phase shift, ϕ, between the two paths the beams will constructively or destructively interfere. A π phase shift destructively interferes the two beams and a 2π phase shift causes constructive interference. The output intensity reflects these sinusoidal interference patterns [2].

$$I_o = \frac{I_i}{2}[1 + cos(\phi)] \tag{1}$$

In this design, an unbalanced MZI configuration is achieved by adding path length, ΔL, to one arm of the interferometer. The propagation constant, β, is the same for both interferometer arms. The transfer function for the design, as a function of wavelength, is shown below.

$$I_o = \frac{I_i}{2}[1 + cos(\beta \Delta L)] = \frac{I_i}{2}[1 + cos(\frac{2\pi n}{\lambda}\Delta L)] \tag{2}$$

B. Ring Resonator

A ring resonator consists of a straight waveguide with a circular waveguide placed next to it. When light travels down the straight waveguide, it evanescently couples into the ring. When the light travels around the loop, it will have a phase shift (ϕ) relative to the light in the straight waveguide. The incoming light from the straight waveguide will constructively or destructively interfere with the light in the ring. The resonance condition, constructive interference, is met when the phase shift is an integer multiple of 2π [3].

$$\phi(\lambda) = \frac{2\pi n_{eff}(2\pi r)}{\lambda} \tag{3}$$

The phase shift (ϕ) for a given wavelength is dependant on the ring radius, r, and effective index of the waveguide.

III. Modeling and Simulation

A. Waveguide Modeling

A strip waveguide, with a width of 500nm and a height of 220nm, was used for all design variations. The waveguide consists of a Si core with a SiO_2 cladding. The mode profile for the primary TE mode at 1550nm was simulated using Tidy3D's mode solver and showed good confinement.

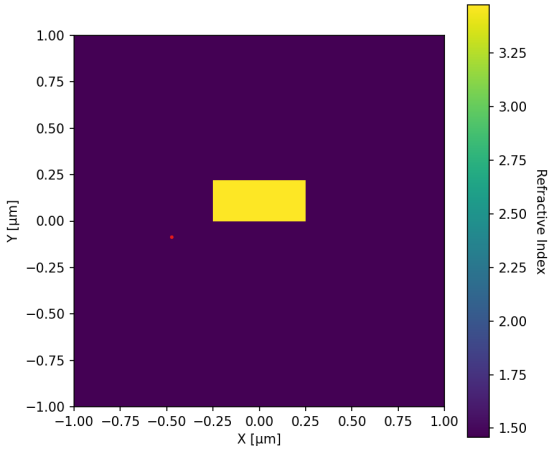

Fig. 1. Cross-section of waveguide index profile.

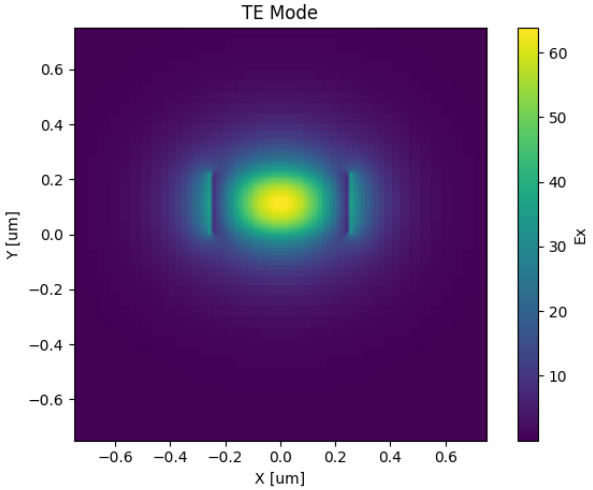

Fig. 2. TE mode profile at 1550nm.

The compact equation of the waveguide can be used to model the effective index of a waveguide as a function of

wavelength. The parameters n_1, n_2, and n_3 are found by fitting equation (3) to $n_{eff}(\lambda)$ simulated using Tidy3D's mode solver.

$$n_{eff}(\lambda) = n_1 + n_2 \cdot (\lambda - \lambda_0) + n_3 \cdot (\lambda - \lambda_0)^2 \quad (4)$$

$$n_{eff}(\lambda_0) = n_1 \quad (5)$$

$$n_g = n_1 - n_2 \cdot \lambda_0 \quad (6)$$

$$D = -2\lambda_0 \frac{n_3}{c} [s/m^2] \quad (7)$$

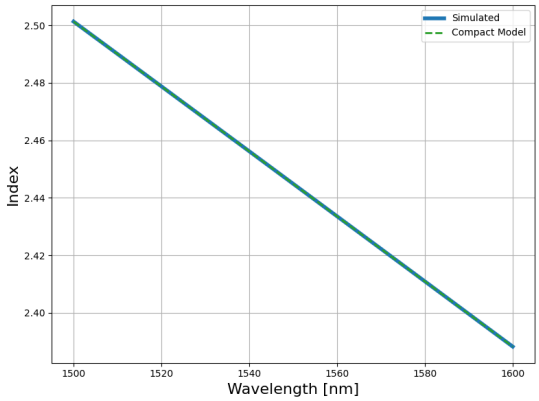

Fig. 3. Compact waveguide model fit to simulated effective index.

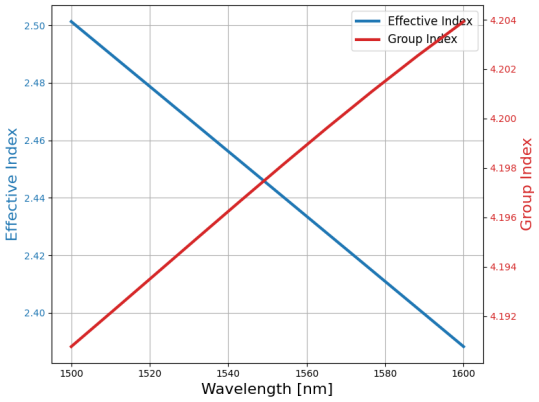

Fig. 4. Effective and group refractive index as a function of wavelength.

B. Device Modeling

For both the MZI and ring resonator devices, three design variations are included on the chip layout. For the MZI, the path delay is altered to achieve different free spectral ranges (FSR). The ring resonator designs have two rings per device to increase the number of design variations on the chip. For each ring, the radius is adjusted to achieve an array of free spectral ranges. Below is the layout of these design variations. The inputs and outputs are coupled into the measurement fiber using grating couplers.

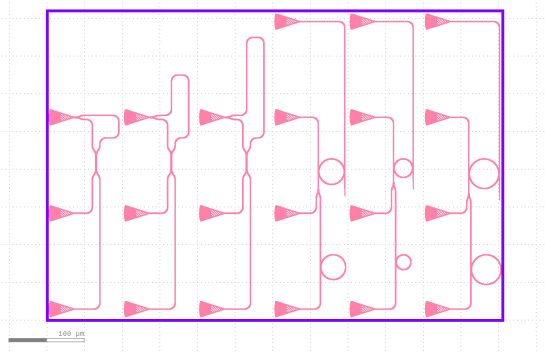

Fig. 5. Chip layout including three MZI devices with different path delays and three ring resonator designs with different radii.

TABLE I
MZI VARIATIONS

Variation	Δ L [um]	FSR [nm]
1	103.6	9.24
2	242.2	3.95
3	408.6	2.34

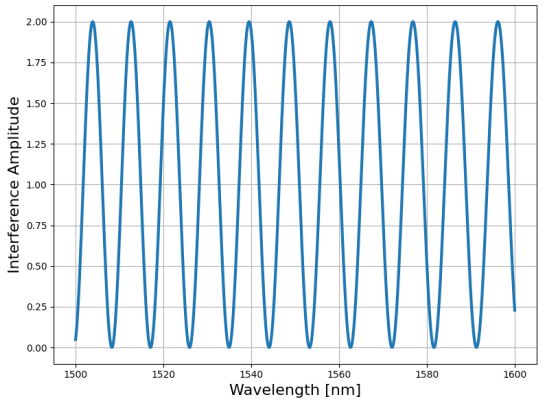

Fig. 6. Simulated interference pattern of MZI design variation No.1.

TABLE II
RING RESONATOR VARIATIONS

Variation	$Radius_1$ [um]	FSR_1 [THz]	$Radius_2$ [um]	FSR_2 [THz]
1	16.91	1.12	16.43	1.16
3	12.28	1.55	9.82	1.94
3	19.65	0.967	19.70	0.965

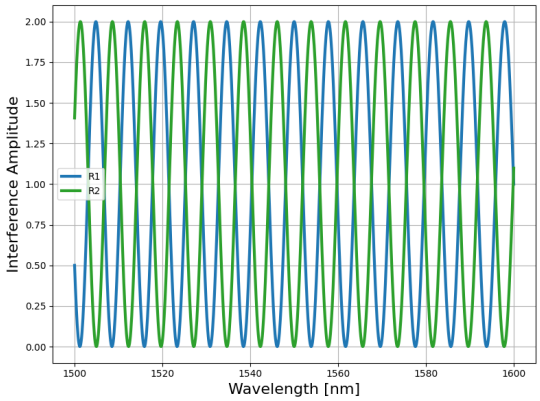

Fig. 7. Simulated interference pattern of ring resonator design variation No.3.

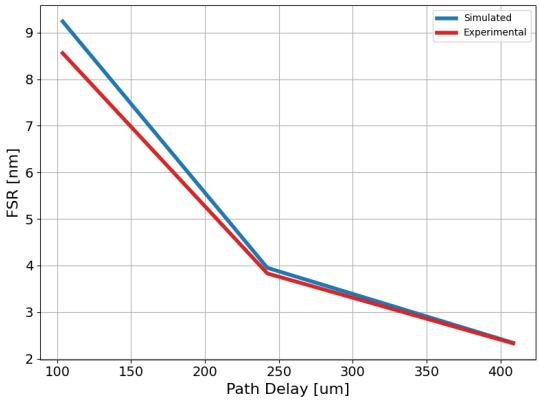

Fig. 9. Variations in path delay and it's effect on real and simulated FSR.

IV. Measurement Analysis

Each device was tested by inputting light at wavelengths spanning from 1500nm-1580nm into a grating coupler and monitoring the output power from the other grating couplers. By analyzing this data, the FSR of both the MZI and ring resonator devices can be calculated.

A. Mach Mach-Zehnder Interferometer

For each device, the FSR from the experimental data was calculated and compared to the simulated results in the following table.

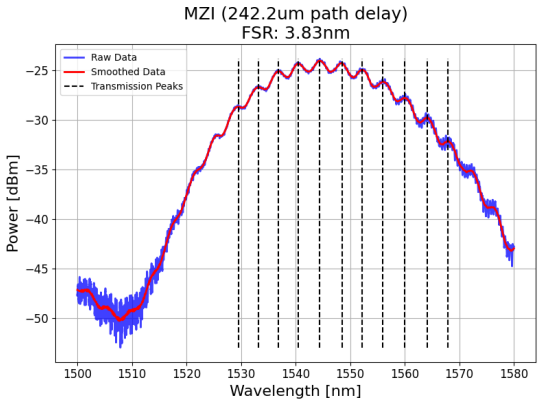

Fig. 8. Test data for MZI device variation No.2 with transmission peaks identified.

TABLE III
MZI Variations

Variation	Δ L [um]	FSR [nm]	FSR_{real} [nm]
1	103.6	9.24	8.56
2	242.2	3.95	3.83
3	408.6	2.34	2.33

The test results are similar to the simulation results. The difference is likely due to manufacturing tolerances and small changes in effective index. The longer the path delay, the more apparent the difference is between theory and experimental data.

B. Ring Resonator

For each device, the FSR from the experimental data was calculated and compared to the simulated results in the following table.

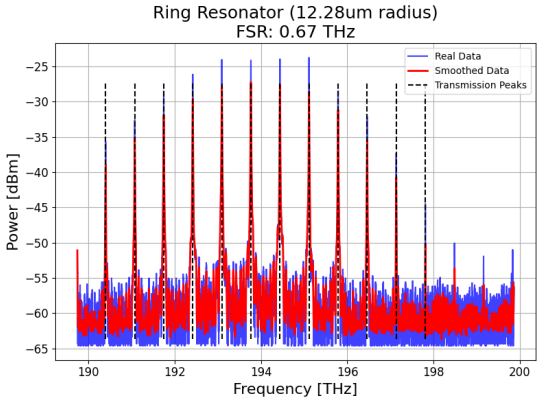

Fig. 10. Test data for ring resonator device variation No.2 with transmission peaks identified.

TABLE IV
Ring Resonator Variations

Variation	$Radius_1$ [um]	FSR_1 [THz]	FSR_{1-real} [THz]
1	16.91	1.12	0.93
3	12.28	1.55	0.67
3	19.65	0.967	0.58

The experimental FSR data does not match the simulations for the ring resonator devices. There is significant error for all design variations and the discrepancy is likely due to an error with the simulation.

V. Conclusion

In this article, several MZI and ring resonator device variations are proposed. The waveguide geometry and mode profile are simulated to confirm confinement. The free spectral range (FSR) is reported for each device variation and is compared to the experimental results. The MZI devices were in agreement with the simulation models, but the ring resonator devices were quite different. The error lies in the simulation results as the difference is significantly more than manufacturing tolerances can account for.

References

[1] R. S. El Shamy, A. E. Afifi, M. M. Badr, *et al.*, "Modelling, characterization, and applications of silicon on insulator loop terminated asymmetric Mach Zehnder interferometer," *Scientific Reports*, vol. 12, p. 3598, 2022.

[2] L. Chrostowski and M. Hochberg, *Silicon Photonics Design: From Devices to Systems*, Cambridge University Press, 2015.

[3] W. Bogaerts, P. De Heyn, T. Van Vaerenbergh, K. De Vos, S. K. Selvaraja, T. Claes, P. Dumon, P. Bienstman, D. Van Thourhout, and R. Baets, *Silicon microring resonators*, Laser & Photonics Reviews, vol. 6, no. 1, pp. 47–73, 2012.